

MODELING THE AUDITORY PATHWAY

A Dissertation

Submitted to the Faculty

of

Purdue University

by

Johannes J. Cilliers

In Partial Fulfillment of the

Requirements for the Degree

of

Master of Science in Electrical and Computer Engineering

May 2009

Purdue University

West Lafayette, Indiana

To Him who is truly nonlinear and time invariant.

## ACKNOWLEDGMENTS

Thank you to Dr. Dhar for direction while I was wandering aimlessly in the parameter space.

Thank you to Dr. Krishnan for providing me the necessary background knowledge of the auditory pathway.

Thank you to the Paramount group for the friendliness and patience extended towards me as a person not familiar with their work.

## TABLE OF CONTENTS

	Page
LIST OF TABLES . . . . .	vi
LIST OF FIGURES . . . . .	vii
ABBREVIATIONS . . . . .	ix
ABSTRACT . . . . .	x
1 INTRODUCTION . . . . .	1
1.1 Background: Problem . . . . .	1
1.2 Objective . . . . .	2
2 BACKGROUND: NEUROSCIENCE . . . . .	4
2.1 Action Potential . . . . .	4
2.2 Auditory Pathway . . . . .	6
2.2.1 Initial Stages . . . . .	6
2.2.2 Auditory Neurons . . . . .	7
2.2.3 Cochlear Nucleus . . . . .	10
2.2.4 Remaining Ascending Pathway . . . . .	11
2.3 Auditory Evoked Potentials . . . . .	12
3 MODELS . . . . .	14
3.1 Auditory Neuron Fiber . . . . .	14
3.2 Spherical Bushy Cell . . . . .	15
3.3 Analysis Tools . . . . .	16
4 NUMERICAL SIMULATIONS . . . . .	18
4.1 Experiment Replication . . . . .	18
4.2 Disorder Modeling . . . . .	23
4.2.1 Polarization and Depolarization Parameters . . . . .	23
4.2.2 Multiple Parameter Changes . . . . .	29

	Page
5 CONCLUSIONS . . . . .	36
6 RECOMMENDATIONS . . . . .	38
LIST OF REFERENCES . . . . .	39
APPENDICES	
A DETAILS OF SPHERICAL BUSHY MODEL . . . . .	42
B ADDITIONAL FIGURES . . . . .	46

## LIST OF TABLES

Table	Page
3.1 Meaning of parameters in spherical bushy cell model. . . . .	16
4.1 Values of the percent change at which drop-offs occur for parameters in SB model. . . . .	27
A.1 Fixed values of parameters in SB model. . . . .	42
A.2 Values of variables that influence the values of parameters in SB model.	43

## LIST OF FIGURES

Figure	Page
2.1 An example action potential where phase I indicates the rising phase, phase II indicates the spiking phase, and phase III indicates the repolarization phase. . . . .	5
2.2 A crude approximation of $A_{BM}$ along the cochlear partition . . . . .	7
2.3 Tuning curves for three AN fibers with CFs of 2 kHz, 4kHz, and 6kHz .	8
2.4 Spike rate of an AN fiber with a CF of 8 kHz in response to a pure tone of 8 kHz . . . . .	9
2.5 The distribution of CFs along a normalized interval . . . . .	10
4.1 The spike rate output of the ten representative AN fibers. . . . .	20
4.2 The result of normalization of the summation of the spike rates. . . . .	21
4.3 A rough approximation of Dau's unitary response. . . . .	22
4.4 The simulated ABR after convolution. . . . .	22
4.5 Spike rate from the AN model and a PSTH from the SB model that have been normalized. . . . .	25
4.6 The PSTHs surrounding a point of interest between a 5% and 10% increase in the value of $C_S$ . . . . .	31
4.7 Results of curve fitting algorithm for respective changes in the value of $C_S$ . . . . .	32
4.8 Changes in scaling factor and delay caused by changes in the value of $C_S$ .	33
4.9 Comparison between scaling factors and delays of $G_{Na}$ and $G_K$ . . . . .	34
4.10 Change in scaling factor and delay of $G_E$ for two different values of $C_S$ .	35
B.1 Changes in scaling factor and delay caused by changes in the value of $G_B$ .	46
B.2 Changes in scaling factor and delay caused by changes in the value of $E_K$ .	47
B.3 Changes in scaling factor and delay caused by changes in the value of $E_{Na}$ .	47
B.4 Changes in scaling factor and delay caused by changes in the value of $G_L$ .	48
B.5 Changes in scaling factor and delay caused by changes in the value of $E_L$ .	48

Figure	Page
B.6 Changes in scaling factor and delay caused by changes in the value of $G_E$ .	49
B.7 Changes in scaling factor and delay caused by changes in the value of $E_E$ .	49

## ABBREVIATIONS

ABR	auditory brainstem response
AC	auditory cortex
AEP	auditory evoked potential
AN	auditory neuron
AP	action potential
AVCN	anteroventral cochlear nucleus
BM	basilar membrane
CF	characteristic frequency
CN	cochlear nucleus
DCN	dorsal cochlear nucleus
EEG	electroencephalogram
LL	lateral lemniscus
MGB	medial geniculate body
MLR	middle latency response
MSO	medial superior olive
PSTH	post-stimulus-time histogram
PVCN	posteroventral cochlear nucleus
SB	spherical bushy
SOC	superior olivary complex

## ABSTRACT

Cilliers, Johannes J. M.S.E.C.E., Purdue University, May 2009. Modeling the Auditory Pathway. Major Professors: Aditya P. Mathur and Rudolf Eigenmann.

There has been much work done to further the knowledge of disorders that affect the auditory pathway. However, current methods of inducing disorders in test animals is very limited. It cannot be done on a neuron by neuron basis, and problems might arise when generalizing results from test animals to humans. The purpose of this work is to address this lack of precision found in the research of the auditory pathway. This work begins to address a solution to this problem by starting to build a complete computational model of the auditory pathway using previously published models. Specifically, a phenomenological model for auditory neurons and a computational model for spherical bushy cells, that were developed independent of each other, were combined into one simulation. The hope of better understanding how disorders affect the auditory pathway is achieved by changing parameters within the models and comparing the outputs. Through experiments that vary parameters from their published values, failure points for parameters are established. Whether those failure points indicate the useful range of the model or show the failure point of an actual neuron is not conclusive at this point. If it does represent the failure of a neuron, then that would be a useful boundary condition that treatments would need to overcome.

# 1. INTRODUCTION

## 1.1 Background: Problem

Researchers have taken many different roads in order to better understand disorders of the auditory pathway. One road has led to discovering some of the causes behind auditory based disorders. A few of these causes that have been investigated deal with ototoxicity [1,2], which is damage done to the ear by a toxin. Much of this research has focused on the damage done to hair cells by certain antibiotics. Another cause that affects many people today is acoustic trauma from overstimulation, and the research ranges from mild trauma that can be reversed [3] to severe trauma with permanent hearing loss [4]. Still other research is being done to investigate causes that are linked to genetics [5,6] and aging [7].

Part of the research into the causes of disorders is understanding the effects a disorder might have. These effects would include damage to either the inner or outer hair cells, changes in hearing thresholds, and frequency resolutions [8]. However, sometimes a disorder can be identified, but the underlying cause or causes are not readily apparent. This may be a result of there being multiple forms of a disorder. For example, tinnitus, which is sometimes described as a ringing in the ear, has at least two explanations for two different types [8,9]. Another example is a correlation between language-based learning disorders and processing of auditory signals at brainstem and cortical levels [10]. Children with some forms of auditory disorders are unable to discriminate rapid acoustic changes in speech. Some children that have been diagnosed with a language-based learning disorder show abnormal encoding of speech stimuli.

This leads into the area of research that attempts to treat these disorders. One type of treatment that has been developed relatively recently is the cochlear implant.

This type of prosthesis is designed to bypass damaged hair cells and stimulate auditory neurons directly with an electrical signal [8]. Auditory training has been shown to improve the ability to discriminate and identify an unfamiliar sound in the case of the children that have difficulty discriminating rapid acoustic changes [11, 12]. Another treatment that is currently being researched and may become an option is gene therapy, which would attempt to treat disorders caused by genetics.

The final area of research to be discussed here is the development of mathematical models to describe the characteristics and phenomenon observed in the auditory pathway. The complexity of these models can range from simple algebraic equations [13] to complex phenomenological [14, 15] or computational models [16–18]. The benefit of using simpler models under correct circumstances is that they are able to deliver decent approximations without an extensive amount of computations. However, the more complex models are able to deliver much more accurate results, but they can be much more computationally expensive.

## 1.2 Objective

The long term goal of this project is to construct and validate a model of the auditory pathway that would have resolution up to the level of the neuron. There would be many benefits to having such a model be a tool to use in research. If parameters for disorders can be appropriately applied to such a model, then it could provide a greater depth of knowledge into the disorder. Also, if a disorder can be appropriately modeled, treatments for that disorder could possibly be applied to the model in a much easier fashion than current methods.

The short term goal of this project is to begin the building process of such a model. The primary method to accomplish this is obtaining and combining models that have already been derived for systems within the auditory pathway. A goal of this modular approach is that no constraints will be placed on the development history of models. This means that models that are combined are not necessarily created by the same

person or group. The reason for this is that better models are expected to be derived in the future. This work would have very little value if, for every new model, it has to be redone completely. Another goal of this work is to explore the complexity created when two complex models are combined.

## 2. BACKGROUND: NEUROSCIENCE

The goal of this chapter is to provide a context for the information given in later chapters. This is accomplished by providing the necessary background knowledge in neuroanatomy and neurophysiology.

### 2.1 Action Potential

One of the facets of this work is the way a neuron communicates with other neurons. The specific method that is focused upon is called the action potential. One significant property of the action potential is called the “all-or-nothing” property. This states that only the occurrence of a spike, not the height of a spike, depends on the strength of a stimulus. This means that a stronger stimulus will not create a larger spike than a weaker stimulus. However, if the stimulus is too weak, then no spike might occur. The conclusion based on this is that as long as a stimulus is able to generate a spike, the same spike will occur [19].

In its resting state, a neuron is polarized at a voltage between -60 mV and -70 mV. This is due to the ion pumps of the neuron that “trade” three  $\text{Na}^+$  located in the cell with two  $\text{K}^+$  ions located outside the cell. This results in a high concentration of  $\text{Na}^+$  ions in the extracellular fluid, and a high concentration of  $\text{K}^+$  ions in the neuron. This pump works against the concentration and voltage gradients that are present. When the neuron is stimulated, some of the  $\text{Na}^+$  ion channels are opened, which allows an increased flow of  $\text{Na}^+$  ions into the cell. This process raises the voltage within the neuron, so this phase of the action potential (AP) is called depolarization. However, this is only a slow rising phase, as shown in phase I in Fig. 2.1, which resembles a capacitor being charged. Once a neuron has been sufficiently depolarized, meaning it reaches a threshold voltage, the  $\text{Na}^+$  ion channels of the neuron open. The

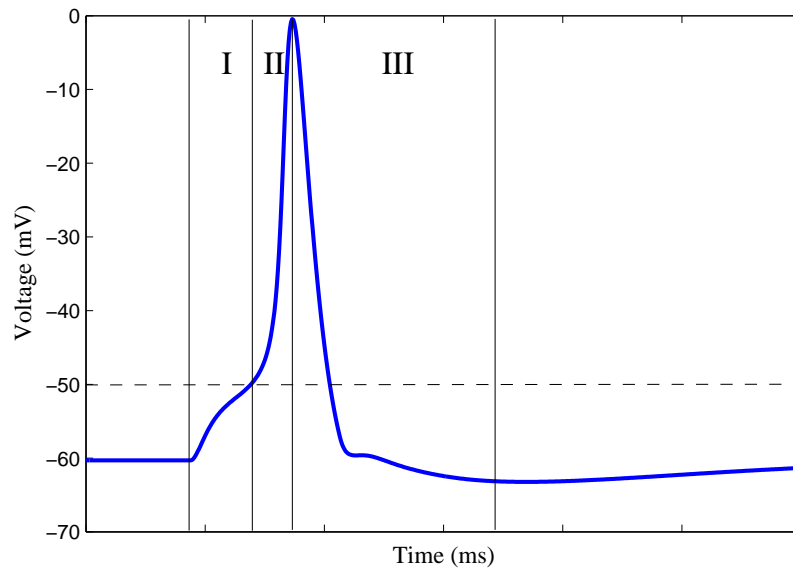


Fig. 2.1. An example action potential where phase I indicates the rising phase, phase II indicates the spiking phase, and phase III indicates the repolarization phase.

threshold voltage usually has a value between -55 mV and -45 mV, but it may be higher if there was a recent enough spike. Due to more  $\text{Na}^+$  ion channels opening, there is a large flow of  $\text{Na}^+$  ions that diffuse into the neuron in order to equalize the concentration and voltage gradients. This is characterized in the action potential as a spiking phase, as shown in phase II in Fig. 2.1, where there is rapid increase in the voltage. At this point the  $\text{K}^+$  ion channels have started opening and the  $\text{Na}^+$  ion channels have started to close. This stops the flow of  $\text{Na}^+$  ions in, and starts the flow of  $\text{K}^+$  ions out of the cell. This is characterized in the action potential as a repolarization phase, as shown in phase III in Fig. 2.1, where the voltage decreases rapidly. Unless interrupted by another stimulus, the voltage will decrease past the resting voltage, and the neuron will be considered to be in a state of hyperpolarization. At this point the  $\text{K}^+$  ion channels close and the ion pump restores the neuron to its resting state [8, 19].

## 2.2 Auditory Pathway

The auditory pathway can be subdivided into two groups based on the direction signals travel. These two groups are labeled as the ascending and descending pathways. Currently, the descending pathway is not focused upon. The reason for this is the desire to slowly increase the complexity of the problem, and attempting to include the descending pathway would add several layers of complexity.

### 2.2.1 Initial Stages

The following is a description of the process of how a sound signal, which is a pressure wave, is transformed into the electrical signal that the neurons in the auditory pathway use in communication with each other.

A sound signal encounters the outer ear and passes through to the middle ear where the signal encounters the Tympanic Membrane. Here the pressure wave's energy is transferred to fluid of the cochlea to create vibrations within the fluid. These vibrations then travel to the basilar membrane (BM) where a wave-like displacement is created.

The BM is usually described in a base to apex fashion. There is an important stiffness gradient that is created because the BM changes from narrow and loose at the base to broad and stiff at the apex. This stiffness gradient is important to the encoding of sound because the frequency of oscillation becomes a function of the position along the BM. In other words, consider the frequency of vibration of the BM to be represented by  $f_{BM}(x)$  for  $x$  on the closed interval  $[b, a]$ , where  $x = b$  is the most basal position and  $x = a$  is the most apical position. This interval is also known as the cochlear partition. As  $x$  increases from  $b$  to  $a$ , the value of  $f_{BM}$  also increases. For the purposes of a simplified discussion, consider the input signal to be that of a pure tone at frequency  $f_S$ , and that the wave-like displacement,  $S$ , oscillates at the same frequency.

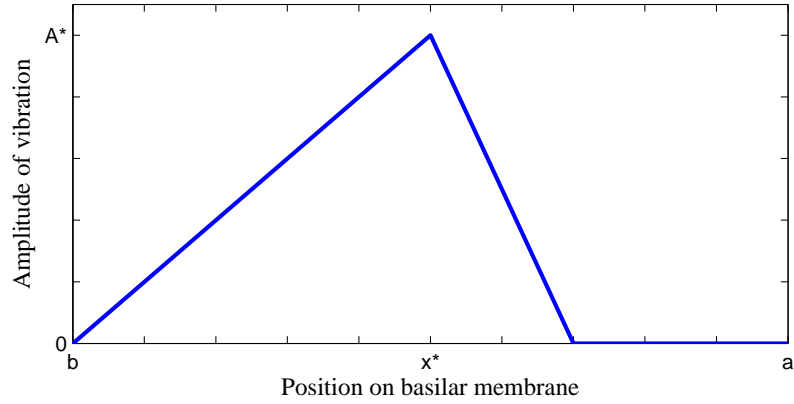


Fig. 2.2. A crude approximation of  $A_{BM}$  along the cochlear partition

This displacement  $S$  is introduced to the BM at the base and travels apically. The amplitude of vibration of the BM depends on the difference between  $f_S$  and  $f_{BM}$ , which will be represented as  $f_d = f_S - f_{BM}$ . Therefore, consider the amplitude of BM vibration to be represented as  $A_{BM}(f_d)$ , and the position where  $f_S = f_{BM}$  and therefore  $f_d = 0$  to be  $x^*$ . Two conclusions can be drawn at this time. First, that  $f_S > f_{BM}$  on the interval  $[b, x^*)$ , and therefore  $f_d$  is positive. Second, that  $f_S < f_{BM}$  on the interval  $(x^*, a]$ , and  $f_d$  is negative. As  $x$  increases from  $b$  to  $x^*$ , where  $f_d > 0$ ,  $A_{BM}$  increases slowly until a maximum is reached at  $x = x^*$ . As  $x$  increases from  $x^*$  to  $a$ , where  $f_d < 0$ ,  $A_{BM}$  is quickly attenuated. A crude approximation of this process is shown in Fig. 2.2.

While the BM is oscillating, hair cells located along the BM transform the mechanical motions of the BM into an electrical signal for the auditory neurons (ANs), which are also referred to as AN fibers.

### 2.2.2 Auditory Neurons

As mentioned above the AN fibers receive input from the hair cells. AN fibers are referred to as having a characteristic frequency (CF). This means that at a particular frequency, the threshold is much lower when compared to other frequencies of the

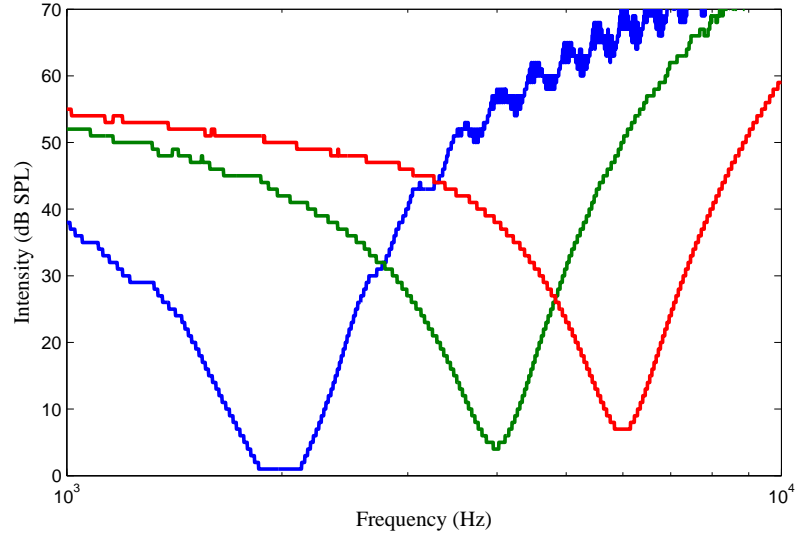


Fig. 2.3. Tuning curves for three AN fibers with CFs of 2 kHz, 4kHz, and 6kHz

same AN fiber, as shown in Fig. 2.3. In this way, AN fibers behave like band-pass filters.

One metric used to describe the response of a neuron is called the spike rate, which is described in units of spikes per second. The spike rate waveform of the AN fibers is describes as a primary-like response. An example of this waveform in response to a pure tone is shown in Fig. 2.4. From this type of response, other response types are formed and compared.

The distribution of CFs along the cochlea is given by Greenwood [20], and he describes the distribution with the equation,

$$CF = A(10^{\alpha x} - k), \quad (2.1)$$

where  $A$  is a constant to yield frequencies in Hertz,  $\alpha$  is a constant that depends on if  $x$  is in millimeters or proportional to the length of the BM,  $x$  is the position of the AN fiber, and  $k$  is an integration constant. The distribution used in this research is shown in Fig. 2.5. The reference points shown are the representative CFs Dau shows in his experiments [21], which will be discussed below. The specific parameter values are not given, so parameters for (2.1) are determined to approximate Dau's reference

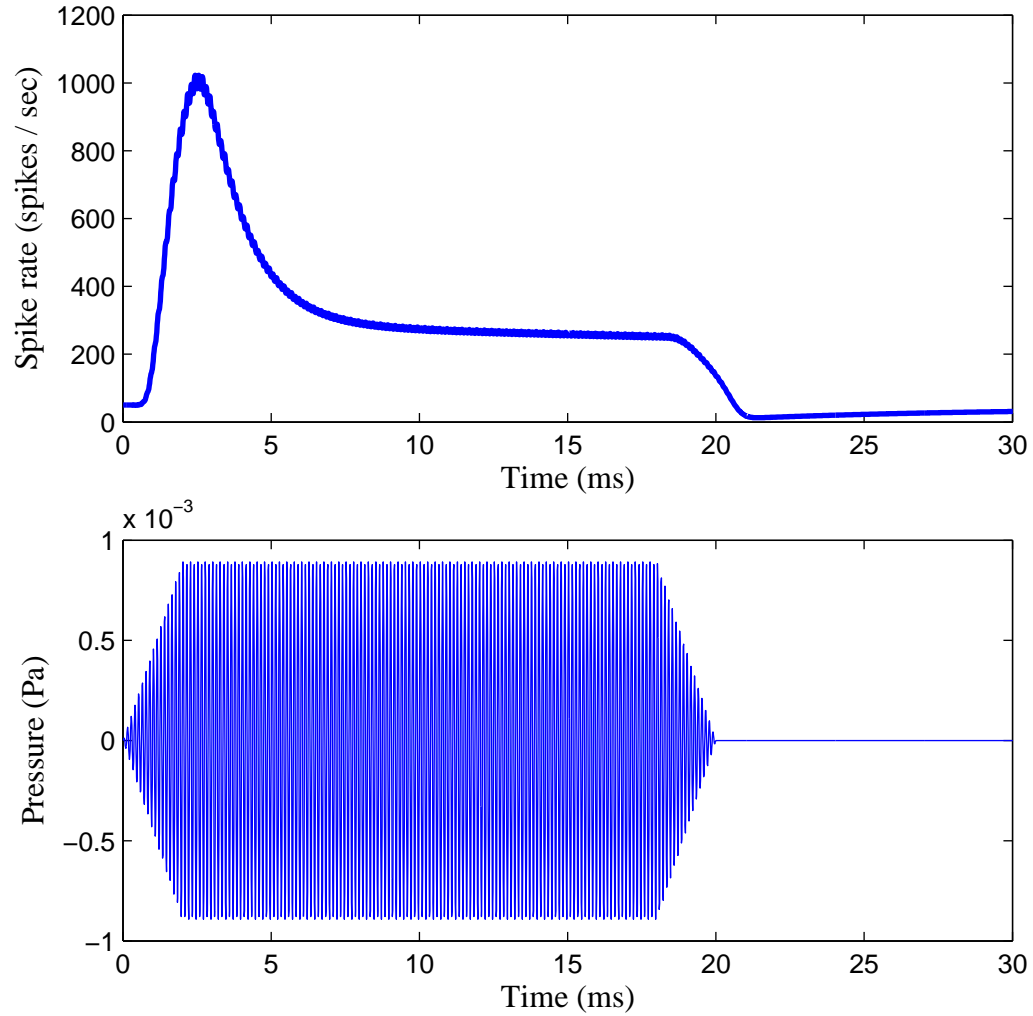


Fig. 2.4. Spike rate of an AN fiber with a CF of 8 kHz in response to a pure tone of 8 kHz

points. The spacing between fibers is assumed to be equal, and are placed on the interval  $[0,1]$  because the units of  $x$  are not known. The parameter values for (2.1) used in this research and shown in Fig. 2.5 are:  $A = 245.4832$ ,  $\alpha = 1.6163$ , and  $k = 0.5924$ .

The AN fibers then pass the signal to the ipsilateral cochlear nucleus.

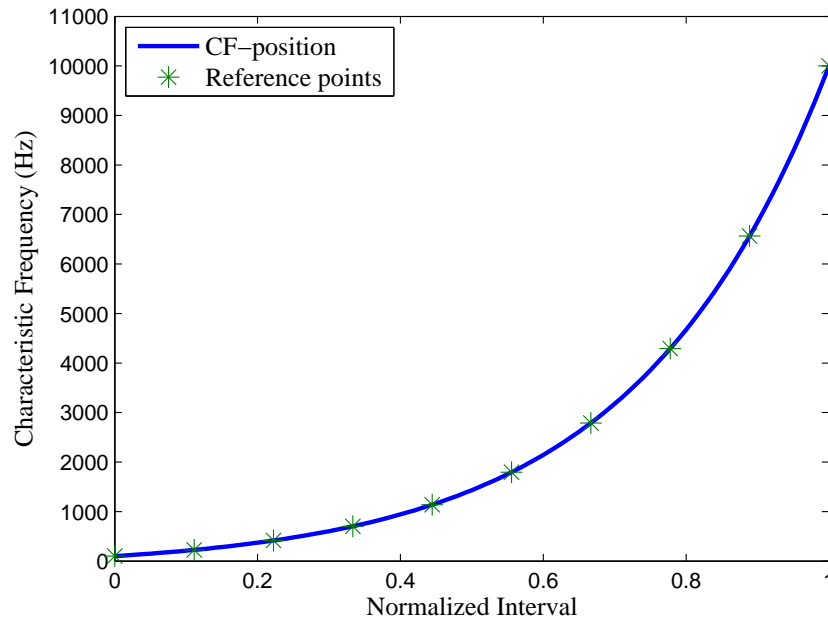


Fig. 2.5. The distribution of CFs along a normalized interval

### 2.2.3 Cochlear Nucleus

AN fibers come into the cochlear nucleus (CN) organized in a tonotopic fashion, and bifurcate upon entering. One path goes through to the dorsal cochlear nucleus (DCN) with projections into the posteroventral cochlear nucleus (PVCN). The other path goes into the anteroventral cochlear nucleus (AVCN). One aspect of complexity of the CN is the different degrees of nonlinearity across these different divisions. If the three divisions were ordered by their degrees of nonlinearity, the DCN would be the most, and the AVCN would be the least. The varying degrees of nonlinearity are the result of the different types of neurons within each division, and whether those neurons receive excitatory or inhibitory. This brings in one aspect of the complexity of the CN, and that is the array of approximately nine different types of neurons within the CN [8, 22]. The AVCN is primarily made up of a type of neuron called a spherical bushy cell.

## Spherical Bushy Cells

As mentioned above, the AVCN is the least nonlinear of the three divisions, and that is because the spherical bushy (SB) cell is the most linear in its response when compared to the other neurons in the CN. Since AN fibers are not perfect in their ability to spike at the correct times, there can sometimes be a “gap” in the output signal. To compensate for this, an average of three AN fibers synapse to one SB cell [8]. The reason for this is that the probability of all the input AN fibers failing to spike is much lower than one AN fiber failing. This redundancy serves to increase the reliability of the SB cell and output a more complete signal to nuclei later in the pathway. Another property of the SB cell that promotes its reliability is the type of synapse it has with the AN fibers. The type of synapse is specifically called an end bulb of Held [8,22], but what is important for this discussion are the properties that are associated with this synapse. These properties are that it is very secure, highly reliable, and has a low synaptic delay. Combining all these properties have the effect of there being high probability that an input spike from an AN fiber is translated into an output spike. This means that the response type of the bushy cell is a primary-like response.

### 2.2.4 Remaining Ascending Pathway

The different divisions do not all output to the same place. The DCN primarily outputs to the contralateral inferior colliculus (IC) with projections to the contralateral lateral lemniscus (LL). The PVCN outputs primarily to the contralateral LL, and the AVCN outputs to the both the ipsilateral and contralateral superior olivary complexes (SOCs).

However, the system considered to be next on the auditory pathway is the SOC. This is where much of the sound localization in the horizontal plane is done. It does this in two ways. One is through the comparison between the arrival times of a signal at both ears. The other is through the comparison between the intensities of

the signal at both ears [8]. The next system is the LL followed by the IC. At the level of the IC there is a significant amount of non-auditory input, such as visual and motor input. The IC passes the signal to the medial geniculate body (MGB), which is located at the level of the thalamus. The system that is considered to be at the end of the auditory pathway is the auditory cortex (AC).

### 2.3 Auditory Evoked Potentials

Before explaining what auditory evoked potentials (AEPs) are, the concept of the electroencephalogram (EEG) must be explained. The human brain is comprised of neurons where roughly  $10^{10}$  of them are active at any given time. The EEG is the recording from the scalp of the aggregate electrical activity from a large population of cortical neurons. The reason the EEG needs to be introduced first is because the AEP is “hidden” within the EEG. The issue with finding the AEP is that its peak value is generally less than that of the EEG peak value, and there are many other neurons not involved with the AEP contributing to the EEG. However, when the brain is stimulated with a sound, a regular waveform occurs within the EEG, which means it consistently has approximately the same shape and time interval after the stimulus. Through techniques such as averaging, the AEP can be extracted from the EEG. The AEP is subdivided into a fast, middle, slow, and late latency response times [19]. However, it should be noted that there is some overlap in the given intervals that they occur in because no exact time can be specified as to when start and stop. This is due to differences from person to person, and the type of stimulus.

The fast latency response is also known as the auditory brainstem response (ABR), and is one of the most common AEPs used in clinics. The ABR is the signal that comprises the first 15–20 ms of the AEP, and is characterized under ideal circumstances by seven peaks labeled I–VII. However, most of the circumstances encountered are less than ideal, so peaks I–V are identified. Also, peaks I, III, and V are considered the most robust of the peaks, and V is generally the largest of the peaks [19]. The

neurons that generate the ABR is still a subject of discussion within the neuroscience community. Some propose that peak I is generated by the spiral ganglion cells of the auditory nerve, III by the SB cells of the AVCN, and V by the principal cells in the medial superior olive (MSO) [21]. The other school of thought on this subject suggests that peak I is generated by the acoustic nerve, II by the CN, III by the SOC, IV by the LL, and V by the IC [23].

The middle latency response (MLR) is characterized as the portion of the AEP from 10–100 ms. This signal is considered to be generated by thalamo-cortical and cortical activity, which corresponds to the neuron activity between the MGB (thalamus) and the AC (cortical) and also the neurons in the AC. The slow latency response is the portion of the AEP from from 50–300 ms and is generated by the cortical level (AC) neurons having a sensory function. Finally, the late latency response is the portion of the AEP from 150–1000 ms and is generated by cortical level (AC) neurons having a processing function [19].

### 3. MODELS

Through the course of this research, many different types of models have been encountered. The following discussion focuses on the models and tools that are in the current implementation of the project.

#### 3.1 Auditory Neuron Fiber

The model used to approximate the AN fibers is a phenomenological model developed by Heinz *et al* [14], and is an extension of the model developed by Zhang *et al* [15]. For this research, an unaltered implementation provided by the Carney Lab of the University of Rochester has been used. The properties that this model sought to replicate are described as compressive changes in gain and bandwidth as a function of stimulus level, changes in the phase of phase-locked responses, and two-tone suppression. The model does not take into account any alteration of the signal due to the properties of ear before the basilar membrane. One of the drawbacks of using a phenomenological model over a computational model, such as the one that will be described in the next section, is that it is difficult to link parameters with their biological counterparts.

There are four main systems working together in this model. The input signal, which is a pressure waveform measured in Pascals, is initially fed into two of these systems that are labeled as the signal path and the feedforward control path. The purpose of the signal path is to approximate the tuning of the basilar membrane. This is done through the use of a time-varying filter in series with a linear filter. The purpose of the control path is to incorporate the compression and suppression effects in AN responses, and to regulate the tuning of the time-varying filter previously mentioned in the signal path. This is done through the use of a wide bandpass filter,

followed by nonlinear saturation, followed by a low-pass filter. Then a function is used to shift and scale the signal based on the fiber’s CF. The output of the control path is then fed back into to the signal path and control path. The output of the signal path is the input to a third system that is labeled IHC-AN synapse. The purpose of the IHC system is to reproduce the transduction properties associated with IHCs. This is done through the use of another nonlinear saturation followed by another low-pass filter. This signal is then passed to the AN synapse model, which contains adaptation properties such the extension of the dynamic range in the transient response as compared to the steady-state response. The output of this system is the spike rate waveform of an AN fiber as a function of time for a given stimulus. This waveform can then be passed to a spike generator system with the purpose of generating instances in time when the AN fiber would discharge and cause a spike. This is done through the use of a nonhomogeneous Poisson process.

### 3.2 Spherical Bushy Cell

The model used to approximate the SB cells is a computational model developed by Rothman *et al* [17] and is an extension of the Hodgkin–Huxley model [16], which approximates the flow of ions across the cell membrane. Dendrites and axons are not incorporated in this model. The central differential equation that Rothman uses is,

$$C_S \frac{dV}{dt} + G_B (V - E_K) + G_K (V - E_K) + G_{Na} (V - E_{Na}) + G_L (V - E_L) + G_I (V - E_I) + G_E (V - E_E) = I_{ext} \quad (3.1)$$

where the meanings of these parameters are outlined in Tab. 3.1. However, several of the parameters are only used in specific experiments that are currently not relevant to this project, and are otherwise set to zero. This model is used after eliminating those parameters,

$$C_S \frac{dV}{dt} + G_B (V - E_K) + G_K (V - E_K) + G_{Na} (V - E_{Na}) + G_L (V - E_L) + G_E (V - E_E) = 0. \quad (3.2)$$

Table 3.1  
Meaning of parameters in spherical bushy cell model.

Parameter	Meaning	Units
$C_S$	membrane capacitance	pF
$G_B$	low-threshold potassium conductance	nS
$E_K$	reversal potential	mV
$G_K$	high-threshold potassium conductance	nS
$G_{Na}$	inactivating sodium conductance	nS
$E_{Na}$	reversal potential	mV
$G_L$	passive leakage conductance	nS
$E_L$	leakage reversal potential	mV
$G_I$	inhibitory synaptic conductance	nS
$E_I$	reversal potential	mV
$G_E$	excitatory synaptic conductance	nS
$E_E$	reversal potential	mV
$I_{ext}$	applied external current	pA

The input to this model is spike times measured in milliseconds, and is fed into the model through  $G_E$ , which is given by,

$$G_E = A_E \frac{t - t_n}{t_p} \exp\left(1 - \frac{t - t_n}{t_p}\right) \quad \text{for } t > t_n \quad (3.3)$$

where  $t_n$  is the arrival time of of the AN spike,  $A_E$  is the input conductance, and  $t_p$  is a constant to vary width of the curve created by an input spike. The detailed equations that define this model are outlined in appendix A.

### 3.3 Analysis Tools

Two main tools are used in this research. The first is a post-stimulus-time histogram (PSTH), which is commonly used in neuroscience research [8,19]. The PSTH

is used to obtain a waveform that will approximate the spike rate of a neuron. This is not needed in the analysis of the AN model because part of the provided output is the spike rate waveform. Therefore, this tool is used to analyze the output of the SB cell model, which has an output of soma potential in millivolts. The general method for obtaining a PSTH is to first stimulate a neuron, which in this case is the input signal from five AN fibers. Then the output spike times are recorded. In this case, a spike is considered to have occurred when an SB cell's potential exceeds  $-25$  mV, and that crossing point is recorded. These two steps are repeated several thousand times. For most of the experiments done for this work, the number of iterations is usually 2000. Next, a time resolution is determined, which is also known as the size of the bin. For this work, a bin size of 0.1 ms is used to give a more general plot of the waveform, and 0.01 ms is used if a point for point comparison is going to be made with the AN model's spike rate output. The array of spike times that was recorded previously is sorted and subdivided by increments of the bin size. The number of spikes that occurs between any two increments is then summed together, and recorded as the spike/bin value of the larger of the two increments.

The other tool is a curve fitting algorithm that uses a particle swarm optimization technique developed by Kennedy and associates [24]. The details of how this technique operates will not be discussed here. This tool is used to find the optimal parameters of an equation or waveform to minimize the difference between two curves. This tool was used to obtain the parameter values of (2.1) to match the reference points given by Dau [21]. In later experiments, this tool is used to find the delay and scaling factor to best match the AN model output with the SB model's PSTH. The detail of these experiments will be described below in greater detail.

## 4. NUMERICAL SIMULATIONS

### 4.1 Experiment Replication

Through the course of this work, certain experiments seemed particularly interesting and possibly relevant to this work. The purpose of this section is to describe efforts to reproduce the results published for an experiment that seems to have a great deal of relevance.

#### Introduction

As previously stated, the ABR is one of the most common tools used in clinics and research. Therefore, it would be useful to be able to reproduce this signal computationally. The effect of changing parameters could be seen and compared with actual data, and ideally such knowledge could lead to improved diagnosis and treatments. That is why the experiment proposed by Dau [21] is appealing to this project. His experiment is centered around producing the ABR using the convolution formula proposed by Melcher and Kiang [25], which is based on the work done by Goldstein and Kiang [26]. A note of importance is that Dau operates under the assumption that peaks I, III, and V are generated by the neural activity of the spiral ganglion of the auditory nerve, SB cells of the AVCN, and the principal cells of the MSO, respectively.

#### Replication

At this point, only reproducing the the results presented by Dau will be done. Due to his inclusion of the MSO and the current lack of MSO models in the project, an extension of Dau's experiment cannot be performed.

Dau used the same AN model developed by Heinz previously discussed. He used 500 AN fibers with CFs that were spaced according to the human cochlear map [20] from 100 Hz to 10 kHz. For this experiment the cochlear map is normalized so that an AN fiber's position is on the closed interval  $[0,1]$  as shown in Fig. 2.5, where a position  $x = 0$  corresponds to 100 Hz and  $x = 1$  corresponds to 10 kHz. From this set of 500 AN fibers, he has ten representative fibers, which are assumed to be equally spaced apart on the cochlear map. These ten representative fibers are the reference points shown in Fig. 2.5.

Dau performs multiple experiments using click and chirp stimuli, but due to the current limited focus of this experiment, only the experiment using the click stimulus at 96 dB SPL will be reproduced. Dau uses an  $80 \mu s$  click stimulus as the input to the set of AN fibers. The click stimulus can be compared to square wave. The benefit of using something similar to a square wave is that it will incorporate all the CFs in the specified range. The spike rate output of the ten representative fibers is shown in Fig. 4.1.

This spike rate information from all the AN fibers is summed together, as shown in Fig. 4.2. The results published by Dau are the summation of the ten representative AN fibers shown in Fig. 4.2(a). The waveform shown in Fig. 4.2(b), which is the summation of all the AN fibers, is what he used in the rest of the experiment.

Next is obtaining the unitary response, but no unitary response has been physically measured for a human. Dau used measured ABRs from click stimuli that were used in a previous study [27]. He deconvolved these signals with the summed spike rate signals, as shown in Fig. 4.2(b), but for the appropriate intensity level. This procedure provides him with a signal that he labels the unitary response. In this case, the procedure on how to obtain the unitary response is not a viable option due to the lack of ABR data. Therefore, a rough approximation of Dau's unitary response, as shown in Fig. 4.3 is made through summation of Gaussian curves with varying means, variances, and amplitudes.

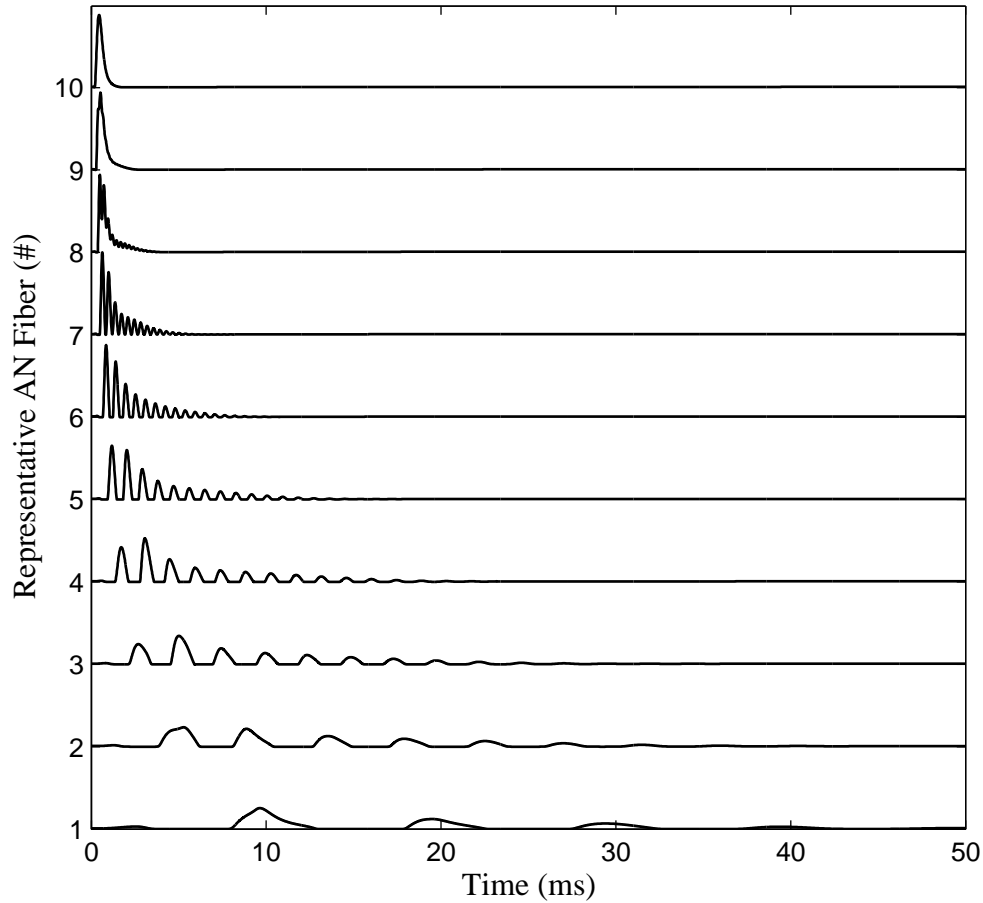
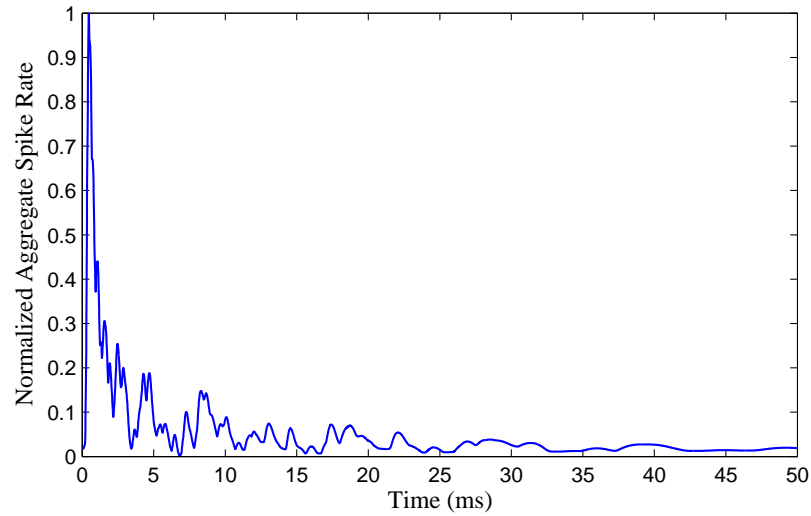


Fig. 4.1. The spike rate output of the ten representative AN fibers.

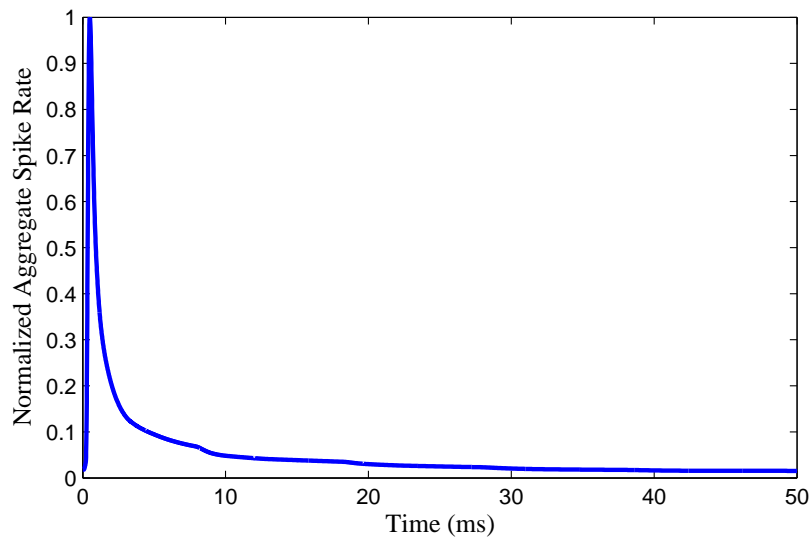
The final step is to convolute the summed spike rate with the unitary response. The results shown in Fig. 4.4 seem to have the typical waveform of an ABR signal.

## Discussion

Error introduced largely from the approximation of the unitary response produces results that are not a perfect replication of Dau's work. However, perfect replication of this experiment is not necessary at this time. This exercise was done to demonstrate a possible way a future model could be beneficial.



(a) The normalized sum of the spike rates of the ten representative AN fibers.



(b) The normalized sum of the spike rates of all 500 AN fibers.

Fig. 4.2. The result of normalization of the summation of the spike rates.

The usefulness of this experiment in the future is contingent on three main factors. First, the assumption on which nuclei generate the peaks of the ABR is correct. This approach might be of little to no use if peak V is proven to be primarily generated by the IC, while this method dictates that it is generated by the SOC. Second, a

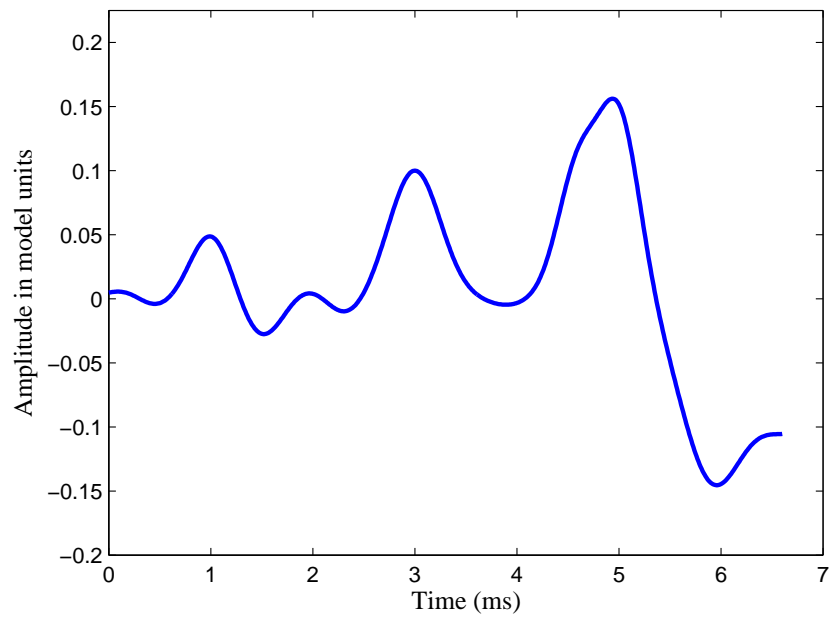


Fig. 4.3. A rough approximation of Dau's unitary response.

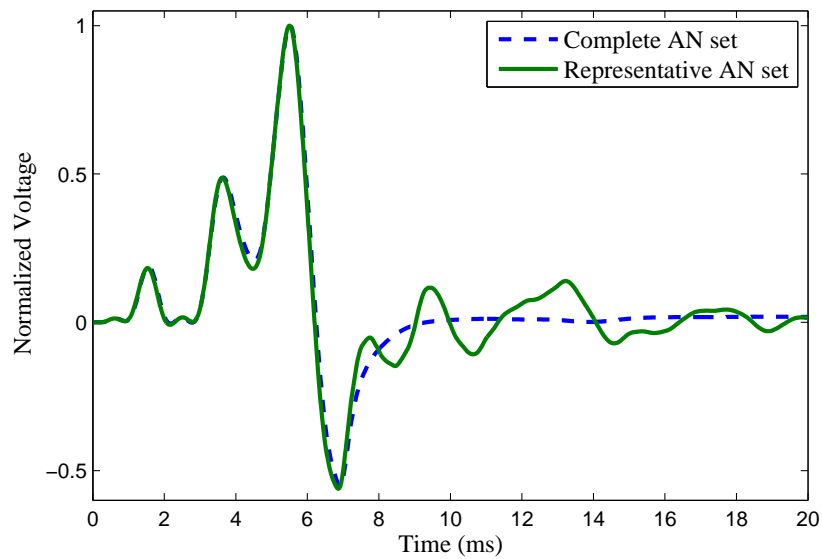


Fig. 4.4. The simulated ABR after convolution.

model, either computational or phenomenological, of the MSO principal cell must be

obtained. This approach cannot be fully explored if at least a third of the necessary signals are missing. Lastly, the unitary response must be derived from the model output. Once again, the unitary response makes up half of the convolution equation, and if that cannot be determined, then this approach cannot be extended.

## 4.2 Disorder Modeling

When discussing disorders of the auditory pathway, it is not necessarily a question of whether a neuron is firing. Rather, it could be a question of how a neuron is firing. This experiment is meant to explore the limits of neuron communication by way of the action potential.

### 4.2.1 Polarization and Depolarization Parameters

#### Introduction

Since the AP is an important part of the communications between neurons, it seems reasonable to presume that an alteration in the AP properties can produce a type of disorder. The problem then becomes changing the properties of the AP. Fortunately, the output of model of the SB cell is soma potential. Also, the SB model is described in terms of ion flow across the cell membrane. The benefit of this setup is that the AP can be split into a depolarization and a polarization phase; each of which can be attributed to the flow of  $\text{Na}^+$  and  $\text{K}^+$  ions, respectively. Therefore, changing the parameters that govern the flow of these ions should alter the AP. However, the SB model contains many other parameters that govern other aspects of the cell, so these will also be investigated.

## Experiment

In order to simplify this initial investigation,  $C_S$  is the parameter chosen to be systematically changed. The reason for this is that in the computational model for the SB cell,  $C_S$  is the parameter that has an affect on all the other parameters.

The parameter values given by Rothman [17] are assumed to be the values for a normal SB cell. Therefore, changes will be made according to this baseline. Since there are differences in the sizes of the values, changes will be made in terms of a percentage of the original value. The assumption made here is that smaller values will require small changes in order to follow changes in the AP, and vice versa for parameters with larger values. The change by percentage results in a incremental change in a parameter that is directly proportional to it's size. To improve the likelihood of being able to observe points of interest and overall trends, a wide, low resolution range of percentage values is selected. The initial range increments by 5% from -40% to +40%. The goal is that based on the results, further analysis can be performed on a smaller range with higher resolution.

The stimulus is a 10  $\mu s$  click at 50 SPL. The AN model is tuned to a CF of 1138 Hz. The reason why this CF is used is because it is a reference CF that was carried over from the replication of Dau's experiment. The following are the steps performed in one iteration,

1. The stimulus is applied to the AN model five times. This is done to replicate the presence of five AN fibers synapsing with the SB cell. The spike time output is sorted and stored in an array each time the stimulus is applied.
2. The spike time array is applied to the SB model, which is implemented using a 4<sup>th</sup> order Runge–Kutta method [28], and the output potential is recorded.
3. From this output, the spike times of the SB cell are computed, and stored in another array.

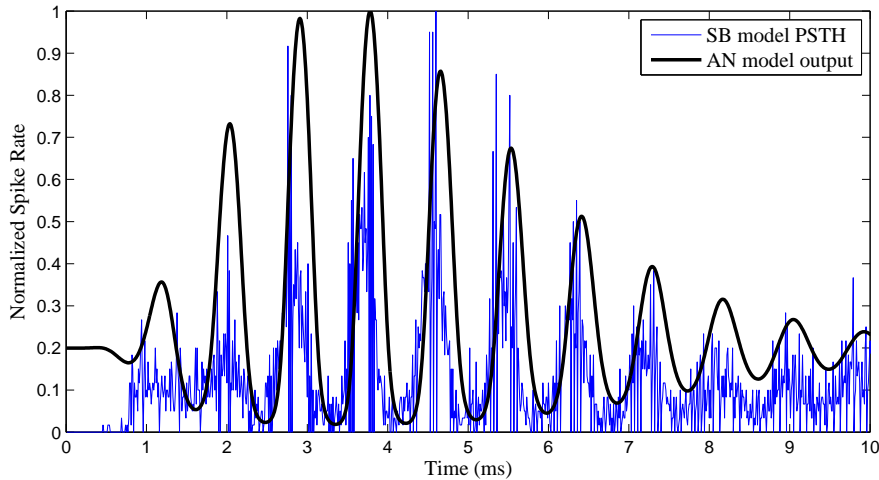


Fig. 4.5. Spike rate from the AN model and a PSTH from the SB model that have been normalized.

4. Steps 1 through 3 are performed for every percentage change of a parameter. A matrix for SB spike times is generated where each row of the matrix corresponds to different percent changes of a parameter.

For the purposes of creating a PSTH, the above steps are repeated for 2000 iterations. The number of columns of the matrix containing the SB spike times increases for each iteration. The resulting PSTH gives a spike rate waveform that is in terms of spikes/bin, with a bin size of 0.01 ms. For all parameters, all the PSTHs are normalized according to the maximum value of the PSTH corresponding to 0% change. The spike rate from the AN model is also normalized to make visual comparisons more effective. The comparison between the outputs are shown in Fig. 4.5, where the PSTH is for 0% change in  $C_S$ .

From inspection of the results for the initial range for changing  $C_S$ , an interesting decrease in the size of the PSTH occurs between 5% and 10% and not for any other interval. Fig. 4.6 shows the PSTHs that result from a 0%, 5%, 10%, and 15% increase in  $C_S$ . The PSTHs for 0% and 15% are included to emphasize the change that has

occurred between 5% and 10%. Also, the difference in the position of the peaks of the 0% and 5% PSTHs is an interesting outcome that will be examined below.

Two additional procedures are developed in order to conduct a more thorough analysis. First, the range of values and step size for the percentage of change is decreased, so the new range starts at 0% and increases by 0.25% up to 15%. Second, a curve fitting algorithm is implemented to find the best parameters to fit the AN model's spike rate waveform to the PSTH of the SB cell. The parameters that are considered in this case are amplitude scaling factor and delay between time of the peaks. The scaling factor is the value by which the normalized AN spike rate must be multiplied by in order to best fit the PSTH. The delay considered here is the amount of time that the PSTH must be shifted by to the left in order to best fit the AN spike rate.

The result of fitting AN spike rates with the SB PSTHs is shown in Fig. 4.7 for a selected group of PSTHs. From the results shown in Fig. 4.8, the point of interest now lies between 6% and 6.25% where there is a sudden decrease, or drop-off, in the height of the PSTH. The trend of the delay is not easily observed in Fig. 4.7, but later analysis will show that unlike the abrupt change in the scaling factor, the trend of the delay is a more gradual increase in the direction of the drop-off.

This process of a broad general range of parameter values followed by more detailed analysis is repeated for all parameters in (3.2).

## Analysis

As previously mentioned, overall trends are not easily observed in figures such as Fig. 4.7. Therefore, the scaling factors and delays are plotted in terms of the percent change of a parameter, as demonstrated in Fig. 4.8. Since much discussion has gone towards the flow of ions, similar curves for  $G_{Na}$  and  $G_K$  are shown in Fig. 4.9.

The figures that show the scaling factor and delay plots for the other parameters are shown in Appendix B. The pieces of information from those figures that are

Table 4.1

Values of the percent change at which drop-offs occur for parameters in SB model.

<b>Parameter</b>	<b>Drop-off</b>	<b>Uncertainty</b>
$C_S$	6.25%	$\pm 0.25\%$
$G_B$	8%	$\pm 1\%$
$G_E$	9%	$\pm 1\%$
$G_K$	19%	$\pm 1\%$
$G_L$	-15%	$\pm 5\%$
$G_{Na}$	-10%	$\pm 0.5\%$
$E_K$	2%	$\pm 0.5\%$
$E_E$	27%	$\pm 1\%$
$E_{Na}$	-20%	$\pm 1\%$
$E_L$	unknown	

necessary for this discussion are the percent values at which the drop-offs occur for each parameter, which is given in Tab. 4.1. The trends for the delays for all the parameters for which a drop-off was determined, are such that they increases in the direction of the drop-off.

One important note is that after the drop-off in the scaling factor, the values for both the scaling factor and the delay become much more sporadic. This is most likely due to there being less of a PSTH signal for the AN spike rate to be fit to. However, finding the locations of the drop-offs is the only analysis done where the specific value of a point is recorded. All other forms of analysis focuses on general trends.

## Discussion

For the results of the change in  $C_S$  values, a possible explanation arises from the fact that  $C_S$  is meant to be a capacitor parameter in the model. When the capacitance

is increased in an RC circuit, which is what the Hodgkin-Huxley model is [16] is based on, the time constant for that RC circuit also increases. This means that the amount of time needed to charge a capacitor to a specified threshold voltage would increase. From the discussion of the AP, that is essentially what is occurring in phase I of Fig. 2.1. However, the effect of the stimulus that starts the process of the AP has a specific duration. As the capacitance of a neuron increases, the situation will be reached where the time necessary to “charge” the AP exceeds the duration of the effect of the stimulus. Combine this with the “all-or-none” property of the AP, and once that situation is reached, a neuron will not be able to reach the spiking stage of the AP for normal stimuli. However, this raises the question of why there are still spikes being recorded in the PSTHs at high  $C_S$  values. The possible explanation for this comes from the fact that there are five AN fibers synapsing this SB cell. If the stimuli from each of these fibers were arranged in a fashion where one was introduced immediately after the other, then the aggregate effect could be characterized as a single stimulus with a much longer duration. However, this type of arrangement is not that common, and that is why there is a drastic decrease, but not an elimination, of the spikes in the PSTH.

A visual comparison between Fig. 4.9(a) and Fig. 4.9(b) shows responses that are essentially mirrored. This would coincide with thinking of these parameters as representing the opposing forces of depolarization and polarization. Although similar drop-offs for  $C_S$ ,  $G_K$ , and  $G_{Na}$  are present, the causes for each are most likely to be different. Since, both  $G_K$ , and  $G_{Na}$  are characterized as conductances, they can also be thought of as the inverse of their respective resistances,  $1/R_K$  and  $1/R_{Na}$ . The other factor in determining the time constant of an RC circuit is the resistance. Similar to the effects of increased capacitance, increasing the resistance, or lowering conductance, will result in longer time constants. First concentrating on  $G_{Na}$ , if it is decreased, then it would increase the time constant, and a similar argument that was made for  $C_S$  can be made here. If  $G_K$  is increased, this would decrease the time constant associated with it. Since the  $K^+$  ions are mainly introduced in phase III of

the AP, increasing it can be seen as introducing phase III earlier in the AP, which would counteract the polarization in phase I and II. Therefore, both decreasing the ability to depolarize,  $G_{Na}$ , and increasing the ability to polarize,  $G_K$ , would counter the polarization in phase I and II of the AP. Also, as similar argument as the one previously stated for  $C_S$  could explain the the decrease, but not the elimination, of the spikes recorded in the PSTH.

Based on the explanations for these three parameters, the characterization of the effect of the other parameters, either polarizing or depolarizing, can be made based on whether the drop-off value is positive or negative.

#### 4.2.2 Multiple Parameter Changes

An effective exploration of the parameter space of the SB model would need to be made in order to understand the interactions among the parameters. The following discussion is a preliminary investigation into these interactions. Based on the previous experiment, an effective exploration could be characterized as defining the drop-off values as relationships between parameters.

For this experiment, the parameters  $C_S$  and  $G_E$  are chosen. The only reason why these two were chosen was because they are not affiliated with a specific ion. The method that is used is similar to the one described in the previous experiment. The only difference is that the value for  $C_S$  is fixed to a different value of 1.06% its original. Since the drop-off value for  $C_S$  was found to be approximately 6% this setup could demonstrate the effects of a neuron near a particular drop-off. The results shown in Fig. 4.10 show the results of how the response changes when the same procedure is taken for two different values of  $C_S$ .

Further exploration of the interactions among parameters would need to be done before any conclusions can be drawn. However, if the results obtained from further experimentation are similar to this preliminary result, then it could corroborate the idea of separating parameters based on polarizing or depolarizing properties. The

possible benefit to being able to classify parameters in such a way, would come into play when attempting to alter the output in a specific way, such as attempting to model a disorder. For example, the properties of the disorder are known to be an increase in response latency and hearing thresholds remain relatively normal. Based on the results in Fig. 4.10, an increase in the value of  $C_S$  by 6% and a decrease in the value of  $E_E$  by 2% would match the properties of the disorder. While an actual disorder would have a much more complicated set of properties and affect more than just the SB cells, the idea remains the same.

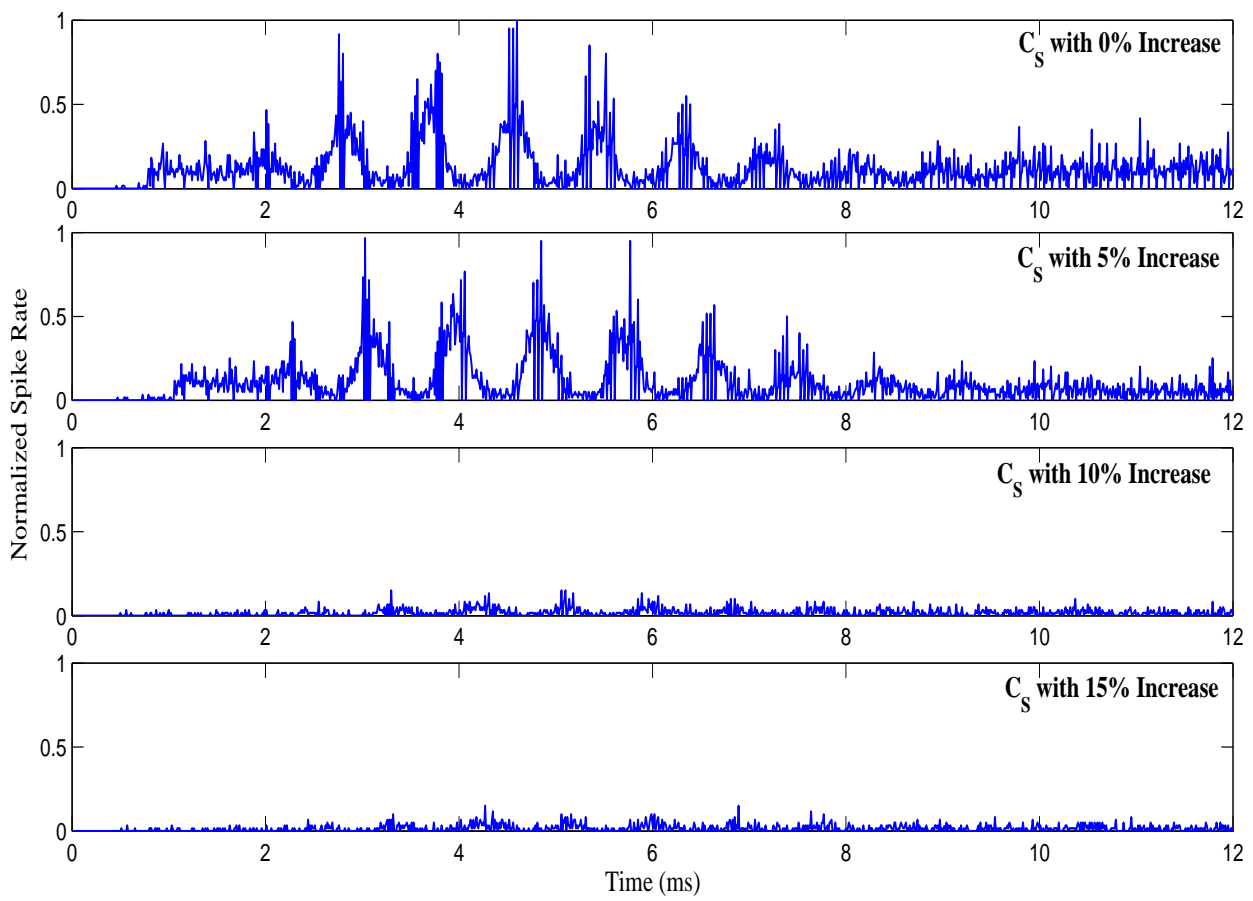


Fig. 4.6. The PSTHs surrounding a point of interest between a 5% and 10% increase in the value of  $C_S$ .

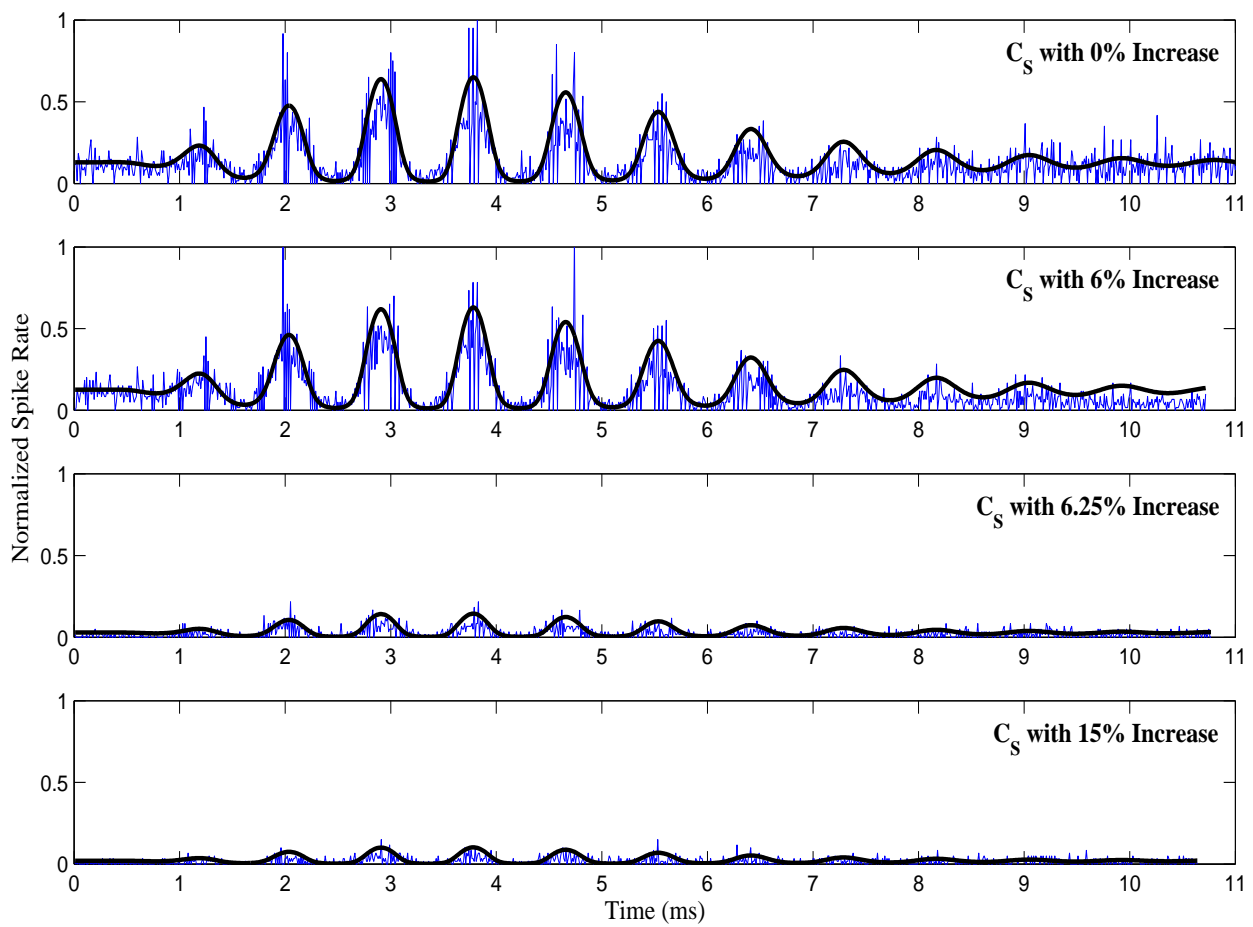


Fig. 4.7. Results of curve fitting algorithm for respective changes in the value of  $C_S$ .

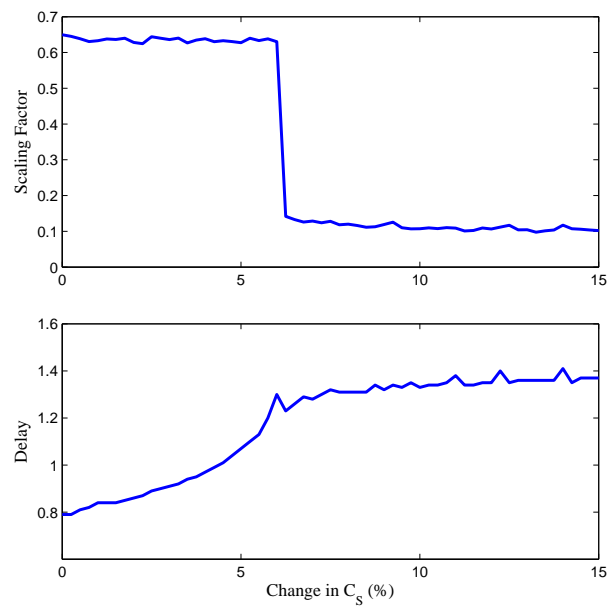
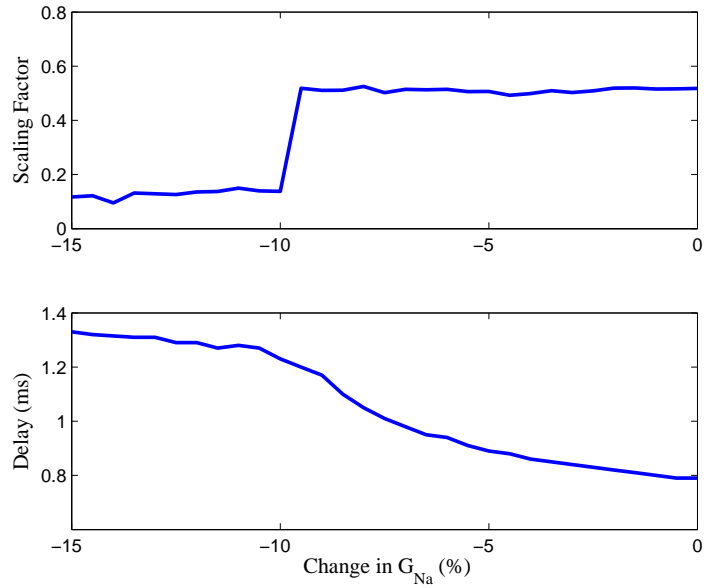
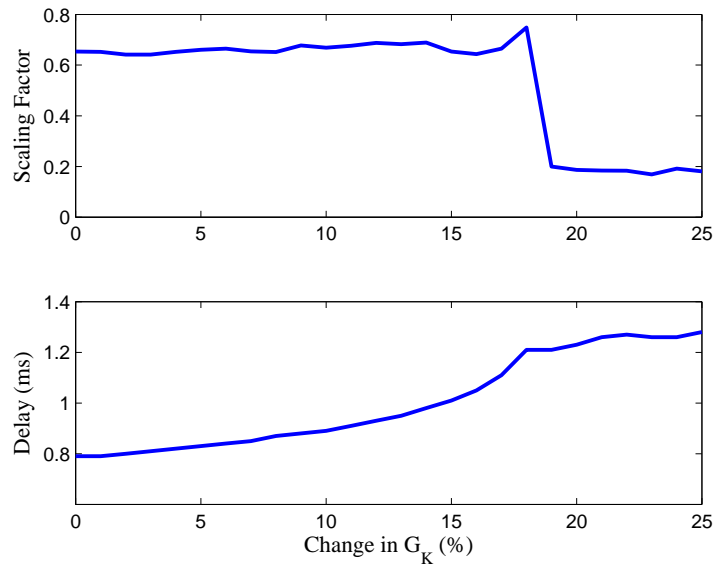


Fig. 4.8. Changes in scaling factor and delay caused by changes in the value of  $C_S$ .



(a) Changes in scaling factor and delay caused by changes in the value of  $G_{Na}$ .



(b) Changes in scaling factor and delay caused by changes in the value of  $G_K$ .

Fig. 4.9. Comparison between scaling factors and delays of  $G_{Na}$  and  $G_K$

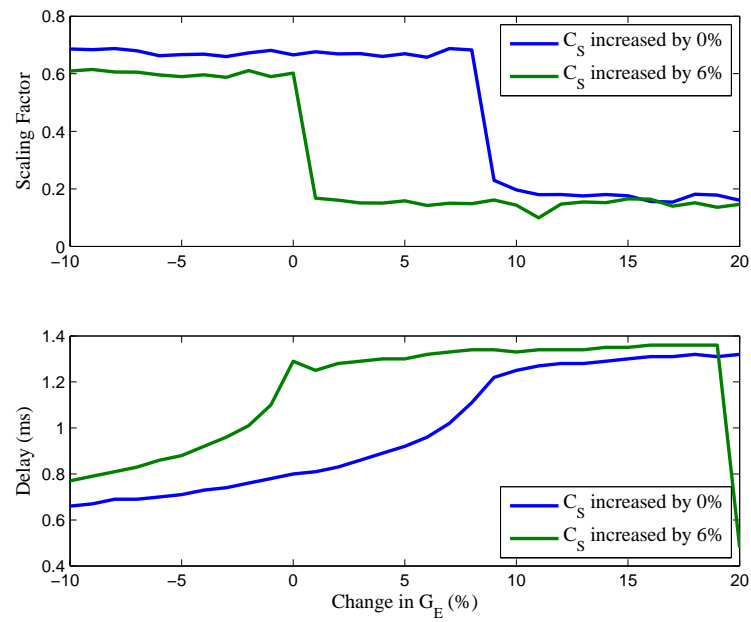


Fig. 4.10. Change in scaling factor and delay of  $G_E$  for two different values of  $C_S$ .

## 5. CONCLUSIONS

The preceding body of evidence is not enough to provide any formal claims, but points toward some possibly interesting findings instead.

The drop-off points could point towards failure points, so the identification of what is failing becomes important. One area of failure could be the implementation of the model. This would be more probable if it occurred for one or two of the parameters, but observing the same phenomenon for all the parameters would seem to make this possibility less and less probable.

Next area of failure could be the model. A failure in the design of the model does not seem likely because these results appear to coincide with the “all-or-nothing” principle of action potentials. This can be compared to rounding a decimal to an integer, where there is a “drop-off” as 0.5 is decreased. Then it becomes a question of whether or not this is a failure of the parameter values of the model. All models of real world functions are unable to match the complex nonlinearities necessary to be a perfect match. However, this obviously does not negate the use of the models, but confines the acceptable accuracy to within ranges of parameter values. The usefulness of the model in a situation is merely determined if the parameter values of present circumstances lie within those ranges. Then the usefulness of this work is that it is beginning to outline these failure points of parameters within the model. This in turn would increase the efficiency of later work because time would not be wasted on accounting for parameter values that do not lie within the useful range of the model.

The other possibility is that these failure points indicate under what circumstances the actual neuron would start to fail. To show that if this is the case, a connection would need to be drawn between the output of these experiments and actual disorders. The disorders that would be characterized by such changes would display certain properties. One would be an “all-or-nothing” property in terms of hearing

thresholds. As the severity of the disorder increases there would be little-to-no discernible attenuation of the thresholds until a certain point where there would be a drastic change in threshold. However, a disorder would still be recognized as being present because the latencies would follow a type of slope as the severity of the disorder increases. If this is the case, then clearly defining these points and their interactions with all the parameters could indicate the boundary conditions that a treatment would need to cross in order to be effective.

## 6. RECOMMENDATIONS

This work has undergone many course changes since it began. Therefore, the following are merely broad stroke suggestions on what would need to be accomplished at some point in the future.

**Explore Parameter Space** - This approach would consist of by mapping the failure points of the parameters, and exploring the interactions between parameters. Also, at this time, Heinz's model has been unaltered. Therefore, another aspect of this approach would be to observe changes in output of the SB model, while parameters of the AN model are changed.

**Vertical Expansion** - This approach would consist of obtaining models for the other nuclei in the auditory pathway. Specifically, finding a model for the principal neurons in the MSO would seem the most advantageous. If such a model were obtained, then an extension of Dau's experiment could be performed.

**Horizontal Expansion** - This approach would consist of improving the efficiency of the current program. Parallelizing the program seems to be a plausible route, but to be an effective route—despite MATLAB's parallelizing feature—the program may need to be rewritten into another programming language such as C, Java, etc, which has shown itself to be problematic in the past.

**Disorder Modeling** - This approach would consist of attempting to obtain a model of a disorder that affects the auditory pathway. The route that seems easiest at this time would be to research a disorder such as multiple sclerosis, which targets neurons in general. The benefit of focusing on such a disorder is that because of its wider area of attack, there may be a larger amount of information available.

## LIST OF REFERENCES

## LIST OF REFERENCES

- [1] A. Forge and J. Schacht, "Aminoglycoside antibiotics," *Audiology & Neuro-Otology*, vol. 5, no. 1, pp. 3–22, 2000.
- [2] E. Hashino, M. Shero, and R. J. Salvi, "Lysosomal targeting and accumulation of aminoglycoside antibiotics in sensory hair cells," *Brain Research*, vol. 777, no. 1-2, pp. 75–85, 1997.
- [3] J. Clark and J. Pickles, "The effects of moderate and low levels of acoustic overstimulation on stereocilia and their tip links in the guinea pig," *Hearing Research*, vol. 99, no. 1-2, pp. 119–128, 1996.
- [4] M. C. Liberman and L. W. Dodds, "Acute ultrastructural changes in acoustic trauma: serial-section reconstruction of stereocilia and cuticular plates," *Hearing Research*, vol. 26, no. 1, pp. 45–64, 1987.
- [5] M. B. Petersen and P. J. Willems, "Non-syndromic, autosomal-recessive deafness," *Clinical Genetics*, vol. 69, no. 5, pp. 371–392, 2006.
- [6] C. Petit, "From deafness genes to hearing mechanisms: harmony and counterpoint," *Trends in Molecular Medicine*, vol. 12, no. 2, pp. 57–64, 2006.
- [7] H. F. Schuknecht and M. R. Gacek, "Cochlear pathology in presbycusis," *Ann Otol Rhinol Laryngol*, vol. 102, pp. 1–16, January 1993.
- [8] J. O. Pickles, *An Introduction to the Physiology of Hearing*. Bingley, UK: Emerald Group Publishing Limited, third ed., 2008.
- [9] J. J. Eggermont, "Tinnitus: neurobiological substrates," *Drug Discovery Today*, vol. 10, no. 19, pp. 1283–1290, 2005.
- [10] B. Wible, T. Nicol, and N. Kraus, "Correlation between brainstem and cortical auditory processes in normal and language-impaired children," *Behavioural Brain Research*, vol. 156, pp. 95–103, 2005.
- [11] N. M. Russo, T. G. Nicol, S. G. Zecker, E. A. Hayes, and N. Kraus, "Auditory training improves neural timing in the human brainstem," *Brain*, vol. 128, pp. 417–423, 2005.
- [12] E. A. Hayes, C. M. Warrier, T. G. Nicol, S. G. Zecker, and N. Kraus, "Neural plasticity following auditory training in children with learning problems," *Clinical Neurophysiology*, vol. 114, pp. 673–684, April 2005.
- [13] M. C. Reed and J. J. Blum, "Model calculations of steady state responses to binaural stimuli in the dorsal nucleus of the lateral lemniscus," *Hearing Research*, vol. 136, pp. 13–28, 1999.

- [14] M. G. Heinz, X. Zhang, I. C. Bruce, and L. H. Carney, “Auditory nerve model for predicting performance limits of normal and impaired listeners,” *Acoustics Research Letters Online*, vol. 2, pp. 91–96, July 2001.
- [15] X. Zhang, M. G. Heinz, I. C. Bruce, and L. H. Carney, “A phenomenological model for the responses of auditory-nerve fibers: I. nonlinear tuning with compression and suppression,” *Journal of the Acoustical Society of America*, vol. 109, pp. 648–670, February 2001.
- [16] A. L. Hodgkin and A. F. Huxley, “A quantitative description of membrane current and its application to conduction and excitation in nerve,” *Journal of Physiology. Lond.*, vol. 117, pp. 500–544, 1952.
- [17] J. S. Rothman, E. D. Young, and P. B. Manis, “Convergence of auditory nerve fibers onto bushy cells in the ventral cochlear nucleus: Implications of a computational model,” *Journal of Neurophysiology*, vol. 70, pp. 2562–2583, December 1993.
- [18] K. L. Levy and D. R. Kipke, “A computational model of the cochlear nucleus octopus cell,” *The Journal of the Acoustical Society of America*, vol. 102, pp. 391–402, July 1997.
- [19] R. F. Burkard, M. Don, and J. J. Eggermont, eds., *Auditory Evoked Potentials: Basic Principles and Clinical Application*. Baltimore, Maryland: Lippincott Williams & Wilkins, 2007.
- [20] D. D. Greenwood, “A cochlear frequency-position function for several species—29 years later,” *Journal of the Acoustical Society of America*, vol. 87, pp. 2592–2605, June 1990.
- [21] T. Dau, “The importance of cochlear processing for the formation of auditory brainstem and frequency following responses,” *Journal of the Acoustical Society of America*, vol. 113, pp. 936–950, February 2003.
- [22] D. B. Webster, A. N. Popper, and R. R. Fay, eds., *The Mammalian Auditory Pathway: Neuroanatomy*. New York, New York: Springer-Verlag, 1992.
- [23] J. A. Winer and C. E. Schreiner, eds., *The Inferior Colliculus*. New York, New York: Springer, 2005.
- [24] J. Kennedy, R. C. Eberhart, and Y. Shi, *Swarm Intelligence*. San Francisco: Morgan Kaufmann, 2001.
- [25] J. R. Melcher and N. Y. S. Kiang, “Generators of the brainstem auditory evoked potential in cat iii: identified cell populations,” *Hearing Research*, vol. 93, pp. 52–71, 1996.
- [26] M. H. Goldstein and N. Y. S. Kiang, “Synchrony of neural activity in electric responses evoked by transient acoustic stimuli,” *Journal of the Acoustical Society of America*, vol. 30, pp. 107–114, February 1958.
- [27] T. Dau, O. Wegner, V. Mellert, and B. Kollmeier, “Auditory brainstem responses with optimized chirp signals compensating basilar-membrane dispersion,” *Journal of the Acoustical Society of America*, vol. 107, pp. 1530–1540, March 2000.

- [28] D. Kincaid and W. Cheney, *Numerical Analysis: Mathematics of Scientific Computing*. Pacific Grove, California: Wadsworth Group, Brooks/Cole, third ed., 2002.

## APPENDICES

## A. DETAILS OF SPHERICAL BUSHY MODEL

The central differential equation that governs the computational model of the spherical bushy (SB) cell, as given by Rothman *et al* [17],

$$C_S \frac{dV}{dt} + G_B (V - E_K) + G_K (V - E_K) + G_{Na} (V - E_{Na}) + G_L (V - E_L) + G_I (V - E_I) + G_E (V - E_E) = I_{ext} \quad (\text{A.1})$$

where the meanings of these parameters are outlined in Tab. 3.1. Some of the parameter values remain constant throughout the simulation, and the values of these parameters at 38°C are given in Tab. A.1,

Some variables in the simulation, such as those listed in Tab. A.2, are directly related to the formulation of certain parameter values.

Table A.1  
Fixed values of parameters in SB model.

Parameter	Value	Units
$C_S$	23	pF
$E_K$	-77	mV
$E_{Na}$	55	mV
$G_L$	5.2	nS
$E_L$	2.8	mV
$G_I$	0	nS
$E_I$	-66.5	mV
$E_E$	-10	mV
$I_{ext}$	0	pA

Table A.2  
 Values of variables that influence the values of parameters in SB model.

Variable	Value	Units
$\overline{G}_B$	86.6	nS
$\overline{G}_K$	173.3	nS
$\overline{G}_{Na}$	985.2	nS

The parameter  $G_E$  is a little more unique in that it can be classified as a piecewise defined function,

$$G_E = A_E \cdot \frac{t - t_n}{t_p} \cdot \exp\left(1 - \frac{t - t_n}{t_p}\right) \quad \text{for } t > t_n, \quad (\text{A.2})$$

where  $A_E$  is the input conductance,  $t_n$  is the AN spike time, and a constant  $t_p = 0.1$ . The reason why  $G_E$  can be classified as a piecewise defined function is that it is strictly non-negative, so when (A.2) results in a negative value, which occurs approximately 0.5 ms after  $t_n$ , it is replaced with a value of zero.

Some of the parameters are dependent on a  $Q_{10}$  temperature correction factor because the original values were measured at 22°C, but need to be corrected for 38°C as follows,

$$G_L = 1.7 \cdot T_f(2)$$

$$\overline{G}_B = 20 \cdot T_f(2.5)$$

$$\overline{G}_K = 40 \cdot T_f(2.5)$$

$$\overline{G}_{Na} = 325 \cdot T_f(2)$$

where  $T_f$  is a function used to impliment the  $Q_{10}$  correction. This function is defined as,

$$T_f(Q_{10}) = Q_{10}^{(T-22)/10},$$

where  $T$  is set to 38°C in this simulation. As previously mentioned, the variables listed in Tab. A.2 are directly related to the formulation of parameters in (A.1) as follows,

$$G_B = \overline{G_B} \cdot w$$

$$G_K = \overline{G_K} \cdot n$$

$$G_{Na} = \overline{G_{Na}} \cdot m^2 \cdot h$$

where the variables  $w$ ,  $n$ ,  $m$ , and  $h$  are defined by the following set of differential equations,

$$\frac{dw}{dt} = \alpha_w \cdot (1 - w) - \beta_w \cdot w \quad (\text{A.3})$$

$$\frac{dn}{dt} = \alpha_n \cdot (1 - n) - \beta_n \cdot n \quad (\text{A.4})$$

$$\frac{dm}{dt} = \alpha_m \cdot (1 - m) - \beta_m \cdot m \quad (\text{A.5})$$

$$\frac{dh}{dt} = \alpha_h \cdot (1 - h) - \beta_h \cdot h \quad (\text{A.6})$$

The variables in (A.3)–(A.6) are then defined as,

$$\alpha_w = \frac{0.107 \cdot T_f(3)}{1 + \exp[-(V + 33)/13.1]}$$

$$\alpha_n = \frac{0.0282 \cdot T_f(3) \cdot (V + 9)}{1 - \exp[-(V + 9)/12]}$$

$$\alpha_m = \frac{0.36 \cdot T_f(3) \cdot (V + 49)}{1 - \exp[-(V + 49)/3]}$$

$$\alpha_h = \frac{2.4 \cdot T_f(3)}{1 + \exp[(V + 68)/3]} + \frac{0.8 \cdot T_f(10)}{1 + \exp[V + 61.3]}$$

$$\beta_w = 0.01881 \cdot T_f(3) \cdot \exp[-(V + 30)/30.3]$$

$$\beta_n = 6 \cdot T_f(3) \cdot \left( \exp[-(V + 144)/30] + \frac{1}{1 + \exp[V + 62]} \right)$$

$$\beta_m = \frac{-0.4 \cdot T_f(3) \cdot (V + 58)}{1 - \exp[(V + 58)/20]}$$

$$\beta_h = \frac{3.6 \cdot T_f(3)}{1 + \exp[-(V + 21)/10]}$$

where  $V$  is the potential governed by (A.1).

The initial values used in this implementation are,

$$V_0 = -60.3076$$

$$w_0 = 0.2035$$

$$n_0 = 0.0154$$

$$m_0 = 0.0112$$

$$h_0 = 0.9598$$

## B. ADDITIONAL FIGURES

The following are the results of the curve fitting algorithm for each parameter in Section 4.2.1.

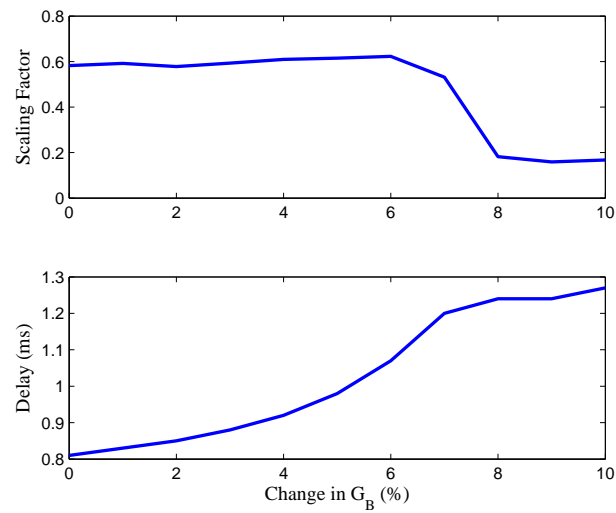


Fig. B.1. Changes in scaling factor and delay caused by changes in the value of  $G_B$ .

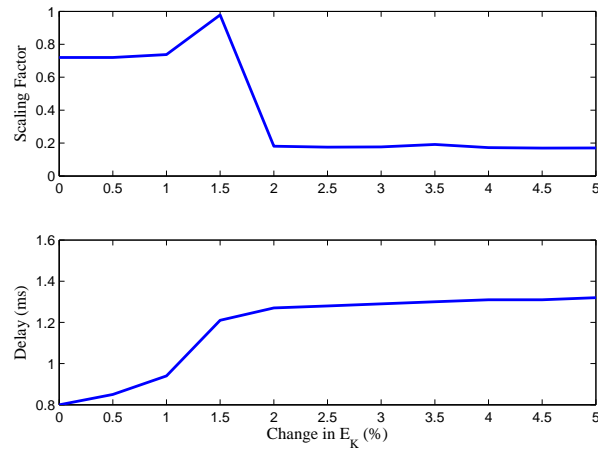


Fig. B.2. Changes in scaling factor and delay caused by changes in the value of  $E_K$ .

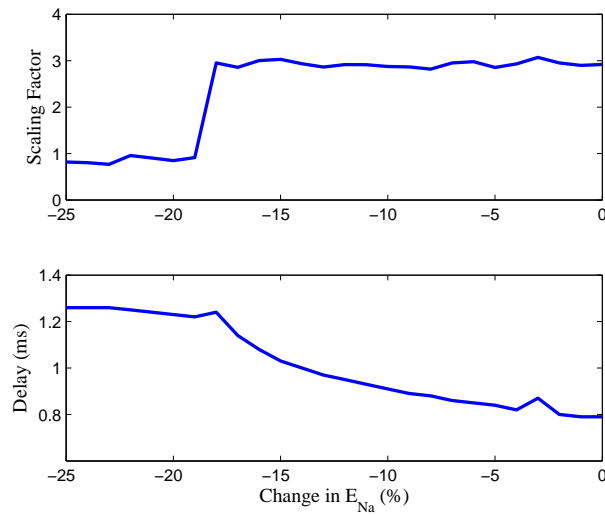


Fig. B.3. Changes in scaling factor and delay caused by changes in the value of  $E_{Na}$ .

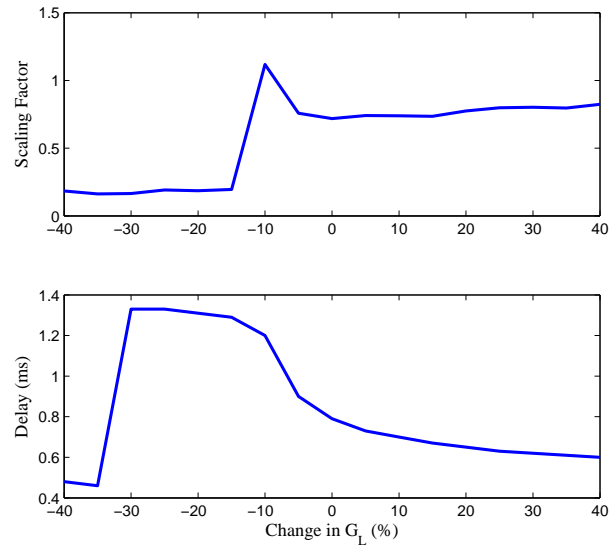


Fig. B.4. Changes in scaling factor and delay caused by changes in the value of  $G_L$ .

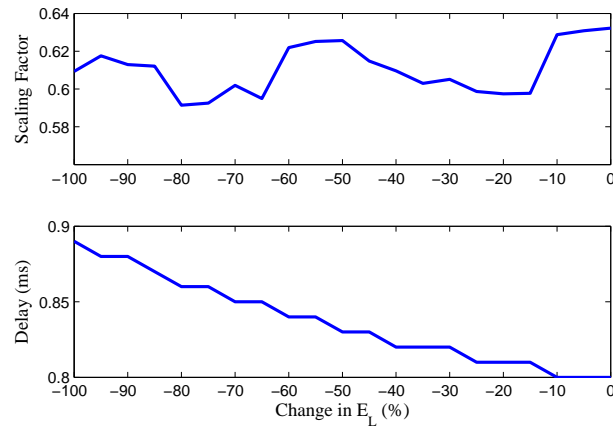


Fig. B.5. Changes in scaling factor and delay caused by changes in the value of  $E_L$ .

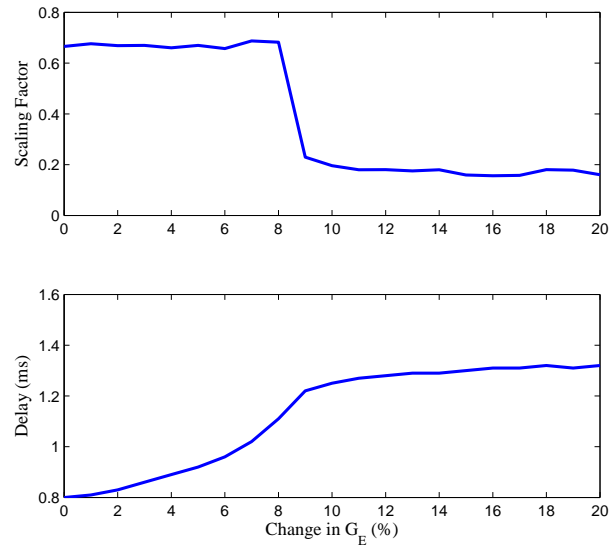


Fig. B.6. Changes in scaling factor and delay caused by changes in the value of  $G_E$ .

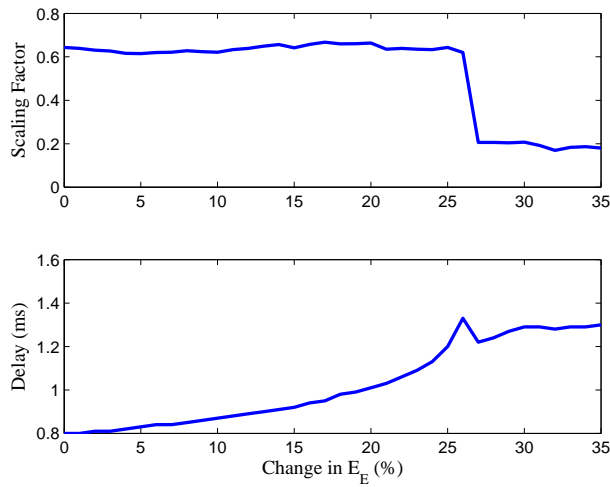


Fig. B.7. Changes in scaling factor and delay caused by changes in the value of  $E_E$ .